# Crystal Structure of a γδ T Cell Receptor Ligand T22: A Truncated MHC-Like Fold

Christer Wingren,[1]* Michael P. Crowley,[2]† Massimo Degano,[1]‡ Yueh-hsiu Chien,[2] Ian A. Wilson[1]§

**Murine T10 and T22 are highly related nonclassical major histocompatibility complex (MHC) class Ib proteins that bind to certain γδ T cell receptors (TCRs) in the absence of other components. The crystal structure of T22$^b$ at 3.1 angstroms reveals similarities to MHC class I molecules, but one side of the normal peptide-binding groove is severely truncated, which allows direct access to the β-sheet floor. Potential γδ TCR-binding sites can be inferred from functional mapping of T10 and T22 point mutants and allelic variants. Thus, T22 represents an unusual variant of the MHC-like fold and indicates that γδ and αβ TCRs interact differently with their respective MHC ligands.**

Classical MHC class I (class Ia) molecules participate in immune responses by presenting peptide antigens to cytolytic αβ T cells (*1*). Many nonclassical MHC class I (class Ib) molecules have distinct antigen-binding capabilities, suggesting that they have evolved for specific tasks that are distinct from those of MHC class Ia (*2*). Although the majority of cells that respond to class Ib ligands express the αβ TCR, the murine H-2T–encoded T22 and the closely related T10 (94% sequence identity) have been identified as specific ligands for two γδ T cell clones, G8 and KN6 (*3–5*). Recognition of T22 and T10 by G8 T cells is fundamentally different from MHC class Ia recognition by αβ T cells (*4–6*). Whereas the MHC class Ia–peptide interaction is essential for both pMHC cell surface stability (*7*) and αβ T cell recognition (*1*), T22 and T10 do not appear to require peptide or any other ligand for cell surface expression or recognition by γδ T cells (*4–6*). Recognition and stimulation are dependent only on a properly folded and stable heterodimer association of the T22 or T10 heavy chain with $\beta_2$-microglobulin ($\beta_2$M) (*4, 6*). *Escherichia coli*–produced T22 and T10 can be refolded in vitro with $\beta_2$M to form a stable heterodimer in the absence of peptide (*6*).

The primary sequences of T22 and T10 suggested that the necessary structural features to bind peptide are absent because of a three–amino acid deletion within the α1 domain, a 13-residue deletion in α2 (*3*), and substitution of four of the eight amino acids that are key for peptide binding by class Ia molecules (*8*). These sequence and structural differences are not shared by other nonclassical and MHC-like molecules, such as CD1 (*9*), H-2M3 (*9*), Zn-$\alpha_2$-glycoprotein (ZAG) (*10*), MIC-A (*11*), hemochromatosis protein HFE (*9*), and the neonatal Fc receptor (FcRn) (*9*). However, these molecules all have modified binding grooves, which are structurally distinct from class Ia proteins, in order to bind alternate ligands such as formylated peptides, glycolipids, and intact proteins (*9–11*). Nevertheless, by comparison, T10 and T22 represent an unusual way for MHC-like molecules to adopt a peptide- or ligand-free structure yet still function in the immune system.

T22 mRNA is expressed by many different cell types in a great variety of tissues similar to MHC class Ia, whereas T10 mRNA is detectable only in cells of the immune system (*3*). Recently, T10 and T22 were demonstrated to be cell activation markers, and a population of T10- and T22-specific γδ T cells was identified in normal mice (*12*). Thus, changes in the level of T10 or T22 expression on cells may act as a trigger for an

**Table 1.** Crystallization, data collection, structure solution, and refinement statistics for T22$^b$. Crystals were obtained by mixing purified T22$^b$ at 13 mg/ml with 0.1 M imidazole-maleate (pH 5.0), 0.2 M calcium acetate, and 10% PEG8000 (*34*). The crystals are orthorhombic $P2_12_12$ ($a$ = 167.1 Å, $b$ = 91.5 Å, $c$ = 122.5Å) with four molecules in the asymmetric unit and a $V_m$ of 2.78 Å$^3$/dalton (*32*). Crystals were flash-cooled to −176°C with 25% glycerol as the cryoprotectant, and data were collected at beamline 9-1 at the Stanford Synchrotron Radiation Laboratory (SSRL) on a MAR image plate detector. Data were integrated and reduced with DENZO and SCALEPACK (*32*). The structure was determined by molecular replacement with truncated coordinates of HLA-A2 (*16, 17*) as the search model. Normalized structure factors from 12.0 to 4.0 Å were used in AMoRE rotation and translation functions and X-PLOR Patterson correlation refinement ($R_{value}$ = 0.47, correlation coefficient = 0.54) (*32*). Phases to 3.1 Å were improved by solvent flattening and fourfold density averaging with DM (final average correlation > 0.85) (*32*). The resulting electron density maps allowed unambiguous rebuilding of the molecule including some previously uninterpretable regions. Multiple rounds of slow-cooled torsion molecular dynamics refinement and model rebuilding were carried out with X-PLOR, CNS, and O (*32*). $R_{free}$ (*32*) was calculated from 3% of the unique data, and only procedures that minimized both $R_{cryst}$ and $R_{free}$ were used. Tight NCS restraints were applied to all regions (rmsd < 0.04 Å), except for two flexible loops involved in lattice contacts (*22*). The final model included 95% of all residues fitted to both averaged and unaveraged $\sigma_A$-weighted $2F_o$-$F_c$ and $F_o$-$F_c$ electron density maps (*32*) and "shake" omit maps (*32*).

| *Data collection statistics* | |
|---|---|
| Resolution range (Å) | 50–3.0 |
| Unique reflections | 34,819 (2597)* |
| $R_{sym}$ (%)† | 8.3 (34.6)* |
| Average $I/\sigma(I)$† | 8.6 (1.6)* |
| Completeness (%) | 90.7 (69.2)* |
| Redundancy | 2.9 (1.8)* |
| *Refinement statistics* | |
| Resolution range (Å) | 20–3.1 |
| $R_{cryst}$† | 0.245 |
| $R_{free}$† | 0.301 |
| Reflections (completeness) | |
| Working set | 29,371 (85%) |
| Test set | 1040 (3%) |
| Number of atoms (Cα) | 11,657 (1430) |
| Average B value (Å$^2$) | 49.4 |

| *rmsd from ideality*‡ | |
|---|---|
| Bond length (Å) | 0.009 |
| Bond angle (°) | 1.5 |
| Dihedrals (°) | 25.9 |
| Impropers (°) | 1.0 |
| *Ramachandran plot*‡ | |
| Favored (%) | 79.1 |
| Allowed (%) | 18.9 |
| Generous (%) | 2.0 |
| Disallowed (%) | 0 |

*Statistics for outer shell of 3.1 to 3.0 Å data are shown in parentheses. †Symbols: $R_{sym} = 100 \times (\Sigma\Sigma|I_i - \langle I\rangle|/\Sigma I_i)$, where $\langle I\rangle$ is the average of equivalent reflections and the sums are extended over all measured observations for all unique reflections. For $I/\sigma(I)$, $I$ is the measured intensity. $R_{cryst} = \Sigma||F_o| - |F_c||/\Sigma F_o$, where $F_o$ and $F_c$ are the observed and calculated structure factors, respectively, and the sum is extended over all unique reflections. For $R_{free}$, the sum is extended over a subset of reflections excluded from all stages of refinement. ‡The rmsd's were calculated with CNS (*32*), and the Ramachandran plot was generated in PROCHECK (*32*).

[1]Department of Molecular Biology and the Skaggs Institute for Chemical Biology, The Scripps Research Institute, 10550 North Torrey Pines Road, La Jolla, CA 92037, USA. [2]Program of Immunology and the Department of Microbiology and Immunology, Stanford University, School of Medicine, Stanford, CA 94305, USA.

*Present address: Department of Immunotechnology, Lund University, Post Office Box 7031, SE-22007 Lund, Sweden.

†Present address: Howard Hughes Medical Institute, Duke Medical Center, Durham, NC 27706, USA.

‡Present address: Structural Biology Laboratory, Sincrotrone Trieste in Area Science Park, S.S. 14 Km 163.5, 34012 Basovizza (TS), Italy.

§To whom correspondence should be addressed. E-mail: wilson@scripps.edu

immunoregulatory γδ T cell function (*12–14*).

To gain further insight into the functions of T10 and T22 and to provide a structural context for understanding γδ T cell–mediated antigen recognition, we determined the crystal structure of $T22^b$ at 3.1 Å. The murine $T22^b$ heavy chain and human $\beta_2M$ heterodimer (*15*) were produced in a soluble form in *E. coli* and crystallized (Table 1). The crystal structure was determined by molecular replacement, with HLA-A2 (*16*, *17*) as a search model (Table 1 and Fig. 1). Four independent copies of $T22^b$ were found in the crystal asymmetric unit.

$T22^b$ adopts an overall MHC-like fold that is structurally more similar to MHC class Ia than to class II and class Ib molecules (*18*) (Figs. 1 and 2). The α chain folds into the standard three domains (α1, α2, and α3) that are closely associated with $\beta_2M$. The relative quaternary arrangement of the α1-α2 platform, α3 domain, and $\beta_2M$ is within the range of orientations observed for MHC class Ia molecules (*19*). The total buried surface area and the number of hydrogen bonds between $\beta_2M$ and the heavy chain are at the lower end of the normal range (*20*) and may explain why the closely related T10-$\beta_2M$ complex is less stable to thermal denaturation than class Ia molecules (*6*). Although the related H-2T–encoded T18 protein is able to bind CD8 (*8*), no data are available on whether T22 can bind CD8. However, most of the MHC class I heavy chain residues of the α3 domain in the CD8-binding site (*16*, *17*) are conserved in $T22^b$ (*21*); the highly acidic loop in α3 is structurally similar to other class I molecules (*21*).

The three–amino acid deletion in the α1 domain (residues 46 to 48) maps to or near the outermost β strand (S4) and the long α helix (H2) of class Ia molecules (*9*). In MHC class Ia (Fig. 1B), the α1 domain has two α-helical segments, named H1 (~ residues 49 to 54) and H2 (~56 to 85) (*9*). $T22^b$ lacks the entire H1 segment and does not start the H2 helical structure until residue 60. Thus, the α1 H2 α helix is substantially shorter in $T22^b$ (Figs. 1 and 2). The conformation of the connecting loop (residues 53 to 59) between S4 and H2 adopts slightly different conformations in the four $T22^b$ monomers, partly because of crystal lattice contacts (*22*) (Fig. 1).

The α2 domain has the least structural resemblance to any known classical or nonclassical MHC-like molecule (*18*) (Fig. 2). This region also displays the greatest structural heterogeneity among nonclassical class I molecules. The 13–amino acid deletion maps to an equivalent region in the α2 domain around the outermost β strand (S4), the loop preceding the first α2 α helix, and the H1 helical segment of class Ia MHC (Fig. 1B), consistent with previous predictions (*3*). Compared with MHC class Ia molecules, $T22^b$ lacks the S4 β strand; the preceding S3 β strand is now connected to the H2a helical segment through an extended chain containing two type IV β turns. The β turns are anchored to the adjacent β strand (S2) by an additional disulfide bond (Cys α110 to Cys α133) that does not occur in any other MHC class Ia or Ib structure (Fig. 1) (*23*). This arrangement may in part account for the COOH-terminal part of S2 being raised 1 to 3 Å compared with class Ia molecules (Figs. 1

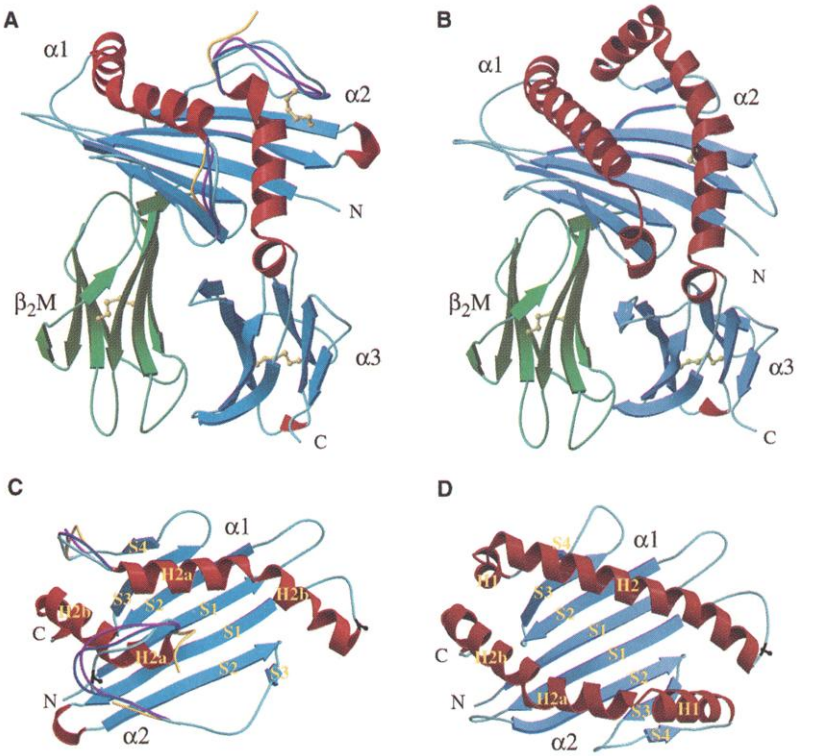


**Fig. 1.** Three-dimensional structures of $T22^b$ and a classical MHC class I molecule (HLA-A2) (*16*, *17*). (**A**) Ribbon diagram of the mouse $T22^b$ heavy chain and human $\beta_2M$ heterodimer. The two loop regions that adopt slightly different conformations in the four $T22^b$ monomers of the asymmetric unit (*22*) are shown and colored yellow, cyan, magenta, and dark blue. No electron density was observed for residues α148 to α153 in molecule 3 (yellow) (*22*). Cysteine side chains (yellow) are shown in a ball-and-stick fashion (*23*). The Asn residues (86 and 150) of probable N-linked glycosylation sites are colored in black [(C) and (D) only]. (**B**) Ribbon diagram of HLA-A2. The molecule is color coded as for $T22^b$ (**C**) Top view of the α1 and α2 domains of $T22^b$. (**D**) Top view of the α1 and α2 domains of HLA-A2. PROMOTIF was used to identify secondary structure elements (*32*). Figures 1, 2, and 3 were generated with MOLSCRIPT (*32*) and RASTER3D (*32*). N, $NH_2$-terminal; C, COOH-terminal.

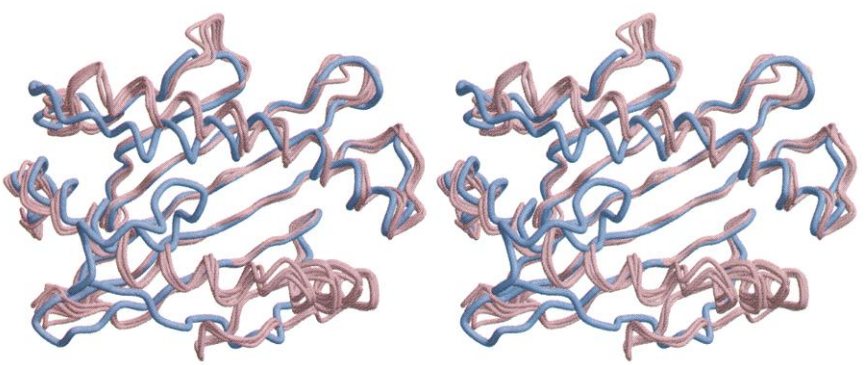

**Fig. 2.** Stereoview comparison of the α1α2 domain of nonclassical murine $T22^b$ (blue) with that of classical human and murine MHC class Ia molecules HLA-A2, HLA-B3501, H-$2K^b$, H-$2D^b$, and H-$2L^d$ (pink) (*9*). The structures are overlapped by superimposition of the β-sheet floor. The β-sheet platform superimposes closely, with the exception of a few loops, whereas there are substantial differences between the helical segments. The overall average rmsd is ~1.6 Å for 70 homologous Cα positions (~0.51 Å for 54 Cα positions). The rmsd values were calculated with SUPPOS (*32*), and DALI (*32*) was used for the structure-based sequence alignment.

and 2). The conformation of the hairpin loop connecting S1 and S2 is also affected. The bulged loop region between S3 and the H2 helices adopts a less well-ordered structure (as indicated by higher than average B values) before it connects to the remnant of the α2 H2a helix; different lattice contacts in the crystal primarily account for the slightly different conformations in the four $T22^b$ monomers (*22*) (Fig. 1). The H2b α2 α helix is conserved as in class Ia molecules (Fig. 1) (*24*). In MIC-A, the α2 α helix segments H1 and H2b are preserved, whereas segment H2a appears to form a flexible, disordered loop region; unlike T22 and T10, MIC-A does not have deletions (*11*).

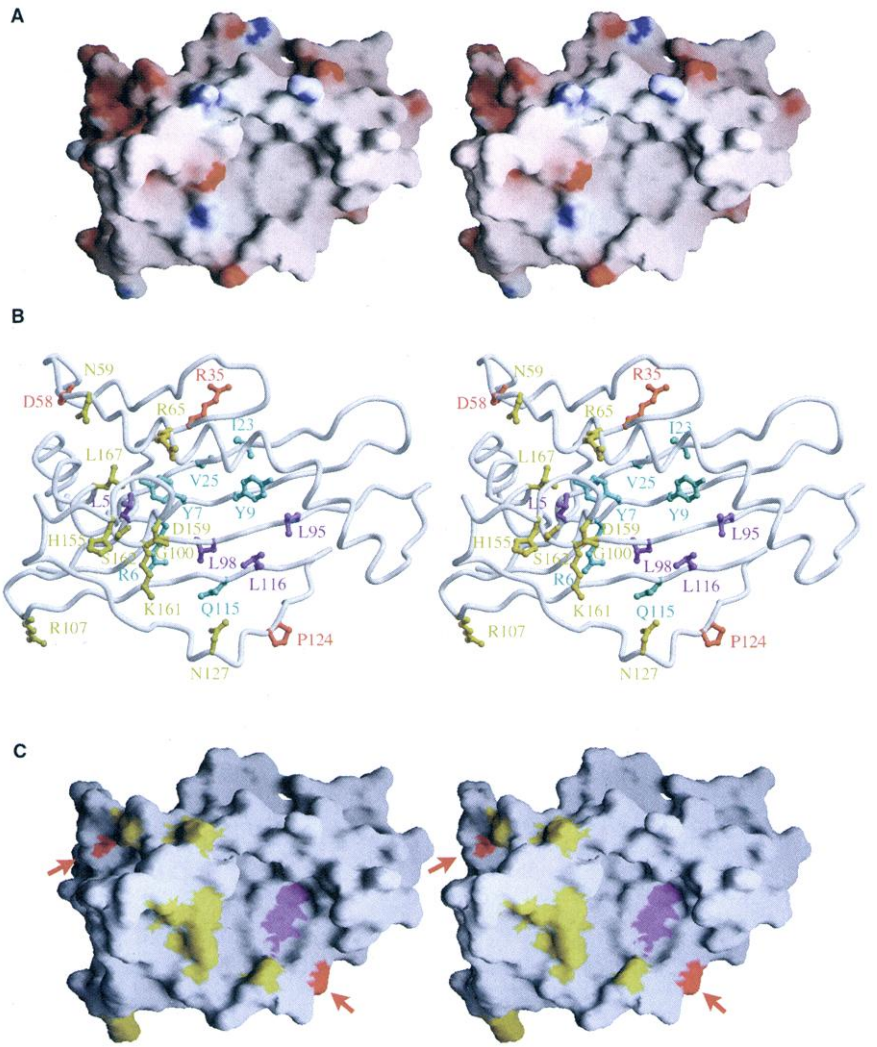


**Fig. 3.** Top view of the α1α2 domains of $T22^b$. (**A**) Stereoview of the molecular surface of the α1α2 domains of $T22^b$. Electrostatic potentials were calculated in GRASP (*32*); positive potential (≥15 mv) is colored blue, neutral potential (0 mv) is colored gray, and negative potential (≤−15 mv) is colored red. (**B**) Stereoview showing potential γδ T cell–binding sites on the α1α2 domains of $T22^b$. G8 and KN6 recognize $T10^b$, $T10^k$, and $T10^{129}$ and $T22^b$ and $T22^{129}$ (*3*, *4*). $T22^k$ and $T22^d$ are not expressed on the cell surface (*3*, *35*); thus, the following amino acid changes are tolerated: $Asn^{59}$ → Asp, $Arg^{65}$ → His, $Gly^{100}$ → Asp, $Arg^{107}$ Gln, $Asn^{127}$ → Ser, $His^{155}$ → Gln, $Asp^{159}$ → His, $Lys^{161}$ → Glu, $Ser^{162}$ → Gly, and $Leu^{167}$ → Val (yellow) (*33*). In contrast, neither G8 nor KN6 recognizes $T10^d$. Antibody staining and surface immunoprecipitation indicate that this molecule is expressed on the cell surface (*35*). Three differences occur in $T10^d$ as compared with $T10^b$ and $T22^b$: $Arg^{35}$ → Leu, $Asp^{58}$ → Gly, and $Phe^{124}$ → His (red). Although one of these mutations could affect the epitope for G8 and KN6, $Asp^{58}$ is on the negatively charged $NH_2$-terminal loop, whereas $Phe^{124}$ is on the exposed β-sheet floor. In addition, KN6 can be stimulated by mutant $T22^b$ molecules with single alanine substitutions at positions $Arg^6$, $Tyr^9$, $Ile^{23}$, $Val^{25}$, or $Gln^{115}$ (green), but not at positions $Leu^5$, $Tyr^7$, $Leu^{95}$, $Leu^{98}$, or $Leu^{116}$ (purple) (*30*). Because $Tyr^7$ normally forms a hydrogen bond with $Gln^{63}$, a mutation at this position is more likely to affect the interaction between the γδ TCR and T22 by secondary effects, such as local disruption of the T22 structure (hence, $Tyr^7$ is colored in green). It is also unclear whether any of these mutant proteins were expressed on the cell surface (*30*). The limited sequence heterogeneity between T22 and T10 is located mainly in the exposed portion of the α1α2 platform; therefore, T10 is predicted to have a closely similar fold to T22. (**C**) Similar to (B), but now displaying the accessible molecular surface. (A) and (C) were generated with GRASP (*32*). The two possible binding sites for the γδ TCR are shown by arrows and emphasize the data obtained from the allelic variants (red).

The relative position of the α1 and α2 helical segments, as well as the curvature of the α1 H2 α helix, differs substantially when compared with class Ia molecules (Fig. 2). The minimum distance between the α1 and α2 helical structures (including the loop preceding the α1 α helix) is only about 6 to 10 Å (Cα to Cα), compared with 12 to 20 Å (class Ia and II), 10 to 13 Å (FcRn), and 7 to 10 Å (MIC-A) (*9*, *11*) for other MHC molecules. The short distance observed in $T22^b$ is mainly a result of the curved α1 α helix, which is more correctly described as a shortened α1 H2 α helix consisting of two segments (H2a and H2b), a feature not yet observed in class Ia molecules (*9*, *24*). The decreased distance between the α1 and α2 α helices creates many noncovalent interactions, including three hydrogen bonds that may substantially stabilize the structure in the absence of ligand. Thus, $T22^b$ adopts a severely modified MHC-like fold that lacks a classical peptide-binding groove (Figs. 1 and 3A), consistent with biological data that indicate that T22 (and T10) do not present peptide for recognition by and stimulation of γδ T cells (*4*–*6*).

Analysis of the electrostatic surface potential reveals the top of the α1α2 domains to be mainly neutral, although a negatively charged patch is present near the $NH_2$-terminal region of the α1 H2a α helix (Fig. 3A). The importance of this patch remains to be elucidated. $T22^b$ has two probable N-linked glycosylation sites at residues 86 and 150 in the α1α2 domains. The first site corresponds to the highly conserved glycosylation site in MHC class Ia molecules, also located at residue 86 (*9*), but the second site is located right in the middle of the protruding loop in the α2 domain (Fig. 1, C and D). Although the *E. coli*–produced $T22^b$ is not glycosylated, we modeled in the carbohydrates to assess their potential functional importance; carbohydrate has been shown to play a role in folding of the heterodimer in MHC class I (α86) (*25*), but not to confer specificity in the $T22^b$-γδ TCR interaction (*6*). However, the carbohydrate bulk may be important in guiding the γδ T cell to its binding site.

Analysis of the length distribution of complementarity-determining region 3 (CDR3) of γ and δ chains indicates more similarity to those of immunoglobulins than to αβ TCRs (*26*). The structural differences between $T22^b$ and MHC class Ia molecules (Fig. 2) further support the idea that γδ and αβ TCRs recognize antigens differently (*4*, *14*, *27*) and that γδ TCRs may be more like immunoglobulins in their recognition properties (*4*, *14*, *28*). Indeed, γδ TCRs are not restricted in their choice of ligands or epitopes. LBK5 γδ T cells recognize

an epitope on MHC class II I-$E^k$, independent of bound peptide and distinct from that recognized by peptide-specific αβ T cells (*4*, *27*). MHC homolog MIC-A has recently been shown to interact with the NKG2D receptor on most γδ T cells, $CD8^+$ αβ T cells, and natural killer (NK) cells (*29*). Structural mapping of MIC-A sequence variations suggests that the potential binding site for the receptor is on the underside of the β-sheet platform (*11*).

To define a potential γδ TCR-binding site on $T22^b$, we mapped allelic sequence differences between T22 and T10 (and two allelic variants thereof) and amino acid substitutions, whose effects on the γδ T cell recognition and activation process are known (*3*, *4*, *30*), onto the crystal structure (Fig. 3, B and C) (*31*). The now exposed β-sheet floor (about 19 Å by 18 Å at the widest dimensions) lies at the base of a deep, hydrophobic cavity, closed on two sides by the α1 H2b and α2 H2a α helices that rise 6 to 10 Å (surface to surface) above the β platform. Two potential interaction sites for the γδ TCR are highlighted on the exposed β-sheet floor and on the acidic patch at the opposite edge of the $T22^b$ surface (red arrows in Fig. 3C) (*31*). Several of these mutations and allelic differences cluster in a patch on the exposed floor and may be a direct contact site for a CDR loop of the γδ TCR. Thus, the crystal structure of $T22^b$ reveals another way for the versatile MHC fold to adapt to a different function in the immune system.

### References and Notes


1. P. J. Bjorkman and P. Parham, *Annu. Rev. Biochem.* **59**, 253 (1990); M. M. Davis *et al.*, *Annu. Rev. Immunol.* **16**, 523 (1998); K. C. Garcia, L. Teyton, I. A. Wilson, *Annu. Rev. Immunol.* **17**, 369 (1999); E. Y. Jones, J. Tormo, S. W. Reid, D. I. Stuart, *Immunol. Rev.* **163**, 121 (1998); G. Mazza *et al.*, *Immunol. Rev.* **163**, 187 (1998).
2. V. M. Braud, D. S. Allan, A. J. McMichael, *Curr. Opin. Immunol.* **11**, 100 (1999); S. M. Shawar, J. M. Vyas, J. R. Rodgers, R. R. Rich, *Annu. Rev. Immunol.* **12**, 839 (1994); I. Stroynowski and K. F. Lindahl, *Curr. Opin. Immunol.* **6**, 38 (1994).
3. M. Bonneville *et al.*, *Proc. Natl. Acad. Sci. U.S.A.* **86**, 5928 (1989); K. Ito *et al.*, *Cell* **62**, 549 (1990).
4. H. Schild *et al.*, *Cell* **76**, 29 (1994).
5. B. C. Weintraub, M. R. Jackson, S. M. Hedrick, *J. Immunol.* **153**, 3051 (1994).
6. M. P. Crowley, Z. Reich, N. Mavaddat, J. D. Altman, Y. Chien, *J. Exp. Med.* **185**, 1223 (1997).
7. D. N. Garboczi, D. T. Hung, D. C. Wiley, *Proc. Natl. Acad. Sci. U.S.A.* **89**, 3429 (1992); M. L. Silver, K. C. Parker, D. C. Wiley, *Nature* **350**, 619 (1991).
8. M. Teitell *et al.*, *Crit. Rev. Immunol.* **14**, 1 (1994).
9. Protein Structures: HLA-A2, Protein Data Bank (PDB) codes 2clr [E. J. Collins, D. N. Garboczi, D. C. Wiley, *Nature* **371**, 626 (1994)], 1hhi [D. R. Madden, D. N. Garboczi, D. C. Wiley, *Cell* **75**, 693 (1993)], and 1akj (*16*); HLA-B8, 1agd, and 1agf [S. W. Reid *et al.*, *J. Exp. Med.* **184**, 2279 (1996)]; HLA-B53 and 1a1o [K. J. Smith *et al.*, *Immunity* **4**, 215 (1996)]; HLA-B3501 and 1a9e [R. Menssen, P. Orth, A. Ziegler, W. Saenger, *J. Mol. Biol.* **285**, 645 (1999)]; H-$2D^d$ and 1bii [A. Achour *et al.*, *Immunity* **9**, 199 (1998)]; H-$2D^b$, 1ce6 [A. Glithero *et al.*, *Immunity* **10**, 63 (1999)], and 1hoc [A. C. Young, W. Zhang, J. C. Sacchettini, S. G. Nathenson, *Cell* **76**, 39 (1994)]; H-$2K^b$ and 2vaa [D. H. Fremont, M. Matsumura, E. A. Stura, P. A. Peterson, I. A. Wilson, *Science* **257**, 919 (1992)]; H-$2L^d$ and 1ldp [J. A. Speir *et al.*, *Immunity* **8**, 553 (1998)]; FcRn, 1frt [W. P. Burmeister, A. H. Huber, P. J. Bjorkman, *Nature* **372**, 379 (1994)], and 3fru [W. P. Burmeister, L. N. Gastinel, N. E. Simister, M. L. Blum, P. J. Bjorkman, *Nature* **372**, 336 (1994)]; CD1 and 1cd1 [Z.-H. Zeng *et al.*, *Science* **277**, 339 (1997)]; H-2M3 and 1mhc [C. R. Wang *et al.*, *Cell* **82**, 655 (1995)]; HFE and 1a6z [J. A. Lebron *et al.*, *Cell* **93**, 111 (1998)]; and I-$A^k$ and 1iak [D. H. Fremont, D. Monnaie, C. A. Nelson, W. A. Hendrickson, E. R. Unanue, *Immunity* **8**, 305 (1998)].
10. L. M. Sanchez, A. J. Chirino, P. J. Bjorkman, *Science* **283**, 1914 (1999).
11. P. Li *et al.*, *Immunity* **10**, 577 (1999).
12. M. P. Crowley *et al.*, *Science* **287**, 314 (2000).
13. R. Boismenu and W. L. Havran, *Curr. Opin. Immunol.* **9**, 57 (1997); S. Porcelli, M. B. Brenner, H. Band, *Immunol. Rev.* **120**, 137 (1991); S. H. Kaufmann, *Proc. Natl. Acad. Sci. U.S.A.* **93**, 2272 (1996).
14. Y. H. Chien, R. Jores, M. P. Crowley, *Annu. Rev. Immunol.* **14**, 511 (1996).
15. Murine T22 is recognized by γδ T cells when paired with either human or mouse $\beta_2$M. Human $\beta_2$M increases the stability of the expressed T10 and T22 heavy chains (*6*), as has been found with murine class Ia MHC H-$2K^b$ [M. R. Jackson, E. S. Song, Y. Yang, P. A. Peterson, *Proc. Natl. Acad. Sci. U.S.A.* **89**, 12117 (1992); M. J. Shields, L. E. Moffat, R. K. Ribaudo, *Mol. Immunol.* **35**, 919 (1998)].
16. G. F. Gao *et al.*, *Nature* **387**, 630 (1997).
17. P. S. Kern *et al.*, *Immunity* **9**, 519 (1998).
18. The program DALI (*32*) was used to search for structurally similar proteins within the PDB. MHC class Ia, class Ib, and class II molecules had the highest similarity scores, as expected. The most similar MHC molecule to $T22^b$ in each MHC class in order of alignment Z score, root mean square deviations (rmsd) for Cα superimposition, and sequence identity is as follows: 20.6, 2.0 Å, and 56% (HLA-B8, PDB code 1agd); 18.4, 2.2 Å, and 58% (H-2M3, PDB code 1mhc); and 14.3, 4.5 Å, and 23% ($IA^k$, PDB code 1iak).
19. $T22^b$ and all MHC class Ia molecules available in the PDB were superpositioned on the basis of the Cα atoms in the β-sheet floor with DALI structure-based sequence alignment (*32*).
20. The total buried surface area and the number of hydrogen bonds between $\beta_2$M and the heavy chain were 845 $Å^2$ and 5 for $T22^b$, whereas the corresponding values for five representative MHC class Ia molecules (PDB codes 1ldp, 2vaa, 1ce6, 1akj, and 2clr) (*9*) were 850 to 1036 $Å^2$ and 7 to 21. HBPLUS (*32*) was used to calculate the number of hydrogen bonds with both distance and geometry criteria. Buried surface areas were computed with MS (*32*) with a 1.4 Å probe, 10.0 spot density, and standard atomic radii.
21. CD8 is bound primarily by amino acids in the α3 domain, including a patch of relatively acidic amino acids at positions 223 to 229. The consensus sequence for these residues in HLA-A, -B, and -C molecules is DQTQDTE (*33*). The corresponding sequence in $T22^b$ is ELTQDME. The rmsd for $T22^b$ and four representative MHC class Ia structures (PDB codes 1akj, 2vaa, 1hoc, and 1ldp) (*9*) was 0.8 to 1.2 Å for residues 223 to 229 and 0.6 to 1.2 Å for residues 220 to 250. Furthermore, three residues in the α2 domain, $Gln^{115}$, $Asp^{122}$, and $Glu^{128}$, are also of vital importance for binding of CD8 (*16*, *17*). Again, these residues are conserved in $T22^b$, and the rmsd for $T22^b$ and MHC class Ia was ~1.9 Å for residues 115 to 128. The values for the rmsd's were calculated with SUPPOS (*32*).
22. No electron density was observed for residues 135 to 140 in molecule 3, nor for the last 18 residues in the heavy chain (part of an extra 20-residue tail added for labeling purposes) in all four molecules. The following residues were truncated to alanines, because of poor electron density for their side chains: molecule 1, $Lys^{170}$ and $Glu^{254}$; molecule 2, $His^{155}$, $Lys^{170}$, and $Glu^{254}$; molecule 3, $Glu^{56}$, $His^{155}$, $Lys^{170}$, and $Glu^{254}$; and molecule 4, $Asn^{126}$, $Lys^{170}$, and $Glu^{254}$. Tight noncrystallographic symmetry (NCS) restraints were applied to all regions except for two extended loop segments, residues 53 to 60 and residues 124 to 159. With molecule 2 as reference, the rmsd values for the first segment were 1.4 to 1.6 Å, and for the second segment they were 2.0 to 2.3 Å (rmsd ≤ 0.3 Å for residues 124 to 126). The differences are primarily due to unique lattice contacts for each molecule and do not appear to be biologically important. The values for the rmsd's were calculated with SUPPOS (*32*).
23. The two disulfide bonds (α101 to α164 and α203 to α259) conserved in all the MHC class Ia structures are present in $T22^b$ as well.
24. The α1 α helix of MHC class Ia molecules is composed of two segments, named H1 (~residues 49 to 54) and H2 (~residues 56 to 85). $T22^b$ lacks helical segment H1. Furthermore, segment 2 is shorter (residues 60 to 86), and it may be more correct to describe it as consisting of two helical segments, residues 60 to 73 (H2a) and residues 74 to 86 (H2b). The rmsd for residues 60 to 86 is ~1.4 Å between $T22^b$ and class Ia molecules (0.4 to 0.8 Å for residues 60 to 73, and 0.5 to 0.8 Å for residues 74 to 86). The α2 α helix of MHC class Ia molecules is composed of three segments, named H1 (~residues 138 to 150), H2a (~residues 153 to 162), and H2b (~residues 164 to 180). $T22^b$ lacks the α2 α-helical segments H1 and most of H2a, whereas the helical segment H2b runs from residues 163 to 180. The rmsd for residues 163 to 180 is ≤ 0.35 Å between $T22^b$ and class Ia molecules.
25. P. Parham, *Trends Biochem. Sci.* **21**, 427 (1996).
26. E. Rock, P. Sibbald, M. Davis, Y. Chien, *J. Exp. Med.* **179**, 323 (1994).
27. J. Hampl *et al.*, *J. Immunol.* **163**, 288 (1999).
28. H. Li *et al.*, *Nature* **391**, 502 (1998).
29. S. Bauer *et al.*, *Science* **285**, 727 (1999); J. Wu *et al.*, *Science* **285**, 730 (1999).
30. S. Moriwaki, B. S. Korn, Y. Ichikawa, L. van Kaer, S. Tonegawa, *Proc. Natl. Acad. Sci. U.S.A.* **90**, 11396 (1993).
31. Comparison of the sequence of $T22^b$ with that of MHC class Ia shows that residues $Arg^6$, $Tyr^7$, $Val^{25}$, and $Arg^{35}$ are highly conserved, whereas residues $Leu^5$ and $Leu^{98}$ are conservative substitutions. In $T22^b$, $Arg^6$ forms a salt bridge with $\alpha Asp^{102}$, $Tyr^7$ forms a hydrogen bond with $\alpha Gln^{63}$ and packs with $Leu^5$, and $Arg^{35}$ forms a salt bridge with $\alpha Glu^{40}$ or $\beta Asp^{53}$. Furthermore, mutation of $Val^{25}$ to a larger residue (Phe) but not to a smaller residue (Ala) will cause the side chain to clash with neighboring residues. Thus, mutation of residues $Leu^5$, $Arg^6$, $Tyr^7$, $Val^{25}$, or $Arg^{35}$ could cause some local disruption of the T22 structure. In fact, a change of $Val^{25}$ → Phe in $T10^b$, which is found naturally in $T22^k$, is known not to be expressed on the cell surface, whereas $Arg^{35}$ → Leu is expressed as deduced from antibody staining and immunoprecipitation (Y. Chien, unpublished results). In addition, the $Leu^5$ → Ala mutant does not stimulate KN6, but the $Arg^6$ → Ala mutant is recognized.
32. X-ray crystallography programs and methods: (i) CNS [A. T. Brünger *et al.*, *Acta Crystallogr. Sect. D* **54**, 905 (1998)]; (ii) X-PLOR [A. T. Brünger, J. Kuriyan, M. Karplus, *Science* **235**, 458 (1987); A. T. Brünger, *X-PLOR*, Version 3.1: *A System for X-Ray and NMR* (Yale Univ. Press, New Haven, CT, 1992)]; (iii) $R_{free}$ [A. T. Brünger, *Methods Enzymol.* **277**, 366 (1997)]; (iv) CCP4 [Collaborative Computational Project No. 4, Daresbury, UK (1994), *Acta Crystallogr. Sect. D* **50**, 760 (1994)]; (v) O [T. A. Jones, S. Cowan, J. Y. Zou, M. Kjeldgaard, *Acta Crystallogr. Sect. A* **47**, 110 (1991)]; (vi) SIGMAA [R. J. Read, *Acta Crystallogr. Sect. A* **42**, 140 (1986)]; (vii) AMoRE [J. Navaza, *Acta Crystallogr. A* **50**, 157 (1994)]; (viii) DENZO and SCALEPACK [Z. Otwinowski and W. Minor, *Methods Enzymol.* **276**, 307 (1997)]; (ix) PROCHECK [R. A. Laskowski, M. W. MacArthur, D. S. Moss, J. M. Thornton, *J. Appl. Crystallogr.* **26**, 283 (1993)]; (x) MS [M. L. Connolly, *J. Appl. Crystallogr.* **16**, 439 (1983)]; (xi) PROMOTIF [E. G. Hutchinson and J. M. Thornton, *Protein Sci.* **5**, 212 (1996)]; (xii) HBPLUS [I. K. McDonald and J. M. Thornton, *J. Mol. Biol.* **238**, 777 (1994)]; (xiii) MERLOT [P. M. D. Fitzgerald, *J. Appl. Crystallogr.* **21**, 273 (1988)]; (xiv) MOLSCRIPT [P. J. Kraulis, *J. Appl. Crystallogr.* **24**, 946 (1991)]; (xv) RASTER3D [E. A. Merrit and M. E. P. Murphy, *Acta Crystallogr. Sect. D* **50**, 869 (1994)]; (xvi) shake omit maps [D. E. McRee, *Practical Protein Crystallography* (Academic Press, San Diego, CA, 1993)]; (xvii) DALI [L. Holm and C. Sander, *J. Mol. Biol.* **233**, 123 (1993)]; (xviii) SUPPOS [F. M. D. Vellieux, DEMON program suite (Grenoble, France)]; (xix) GRASP [A. Nicholls, K. A. Sharp, B. Honig, *Proteins Struct. Funct. Genet.* **11**, 281 (1991)]; (xx) Matthews' coefficient ($V_m$)

[B. W. Matthews, *J. Mol. Biol.* **33**, 491 (1968)]; and (xxi) DM [K. Cowtan and P. Main, *Acta Crystallogr. Sect. D* **54**, 487 (1998)].
33. Single-letter abbreviations for the amino acid residues are as follows: A, Ala; C, Cys; D, Asp; E, Glu; F, Phe; G, Gly; H, His; I, Ile; K, Lys; L, Leu; M, Met; N, Asn; P, Pro; Q, Gln; R, Arg; S, Ser; T, Thr; V, Val; W, Trp; and Y, Tyr.
34. The soluble mouse T22$^b$ heavy chain and human $\beta_2$M heterodimer complex was produced in *E. coli* and purified as described (*6*). The T22$^b$ preparation was then concentrated to 13 mg/ml and extensively dialyzed against 20 mM Hepes (pH 7.2) and 25 mM sodium chloride before crystallization.
35. M. P. Crowley and Y. Chien, data not shown.
36. We thank J. Speir for critical reading of the manuscript and helpful discussions; R. Stanfield, S. Greasley, and A. Heine for help with data collection and data processing; and the staff of SSRL beamline 9-1. This study was supported by NIH grants CA58896 (I.A.W.) and AI33431 (Y.C.), postdoctoral fellowships from the Swedish Foundation for International Cooperation in Research and Higher Education (C.W.), the Foundation BLANCEFLOR Boncompagni-Ludovisi, nee Bildt (C.W.), and an NSF predoctoral fellowship (M.C.). Coordinates have been deposited in the PDB with accession code 1c16.

21 July 1999; accepted 15 November 1999

# A Population of Murine γδ T Cells That Recognize an Inducible MHC Class Ib Molecule

**Michael P. Crowley,[1]* Aude M. Fahrer,[2]† Nicole Baumgarth,[3] Johannes Hampl,[2]‡ Ines Gutgemann,[2]§ Luc Teyton,[4] Yueh-hsiu Chien[1,2]‖**

**Although γδ T cells are implicated in regulating immune responses, γδ T cell–ligand pairs that could mediate such regulatory functions have not been identified. Here, the expression of the major histocompatibility complex (MHC) class Ib T22 and the closely related T10 molecules is shown to be activation-induced, and they confer specificity to about 0.4% of the γδ T cells in normal mice. Thus, the increased expression of T22 and/or T10 might trigger immunoregulatory γδ T cells during immune responses. Furthermore, the fast on-rates and slow off-rates that characterize this receptor/ligand interaction would compensate for the low ligand stability and suggest a high threshold for γδ T cell activation.**

αβ and γδ T cells contribute differently to host immune defense. Mice deficient in γδ T cells generally exhibit more profound defects in the regulation of immune function than in the clearance of intracellular pathogens (*1*). However, neither the ligands nor a normal population of γδ T cells responsible for mediating such immunoregulatory functions have been identified in any of the systems studied.

The closely related nonclassical MHC class I molecules T10 and T22 (94% amino acid identity) have been identified as ligands for two independently isolated γδ T cell clones KN6 and G8 (*2, 3*). T10-$\beta_2$-microglobulin ($\beta_2$M) and T22-$\beta_2$M heterodimers do not bind peptide and adopt a structure distinct from that of classical MHC molecules (*4, 5*). Both heterodimers are recognized directly by G8, without a requirement for other component (*3, 4*). Lipopolysaccharide (LPS)– or concanavalinA (conA)–activated splenocytes stimulate G8 and KN6 better than resting cells (*6*), implying that activation of lymphocytes results in increased expression of T10 and/or T22 on the cell surface. To monitor T10 and T22 expression and to understand its relationship to γδ T cells, we generated a monoclonal antibody (mAb), 7H9, specific for T10 and T22 (*7*). The 7H9 mAb recognizes in vitro folded T10-$\beta_2$M, T22-$\beta_2$M proteins and stains T10 and T22 transfected cell lines [CHO-T10 and T2-T22 (*8*)], but not cells transfected with the MHC class I molecule L$^d$ or the MHC class II molecule I-E$^k$ (Fig. 1A) (*9*). Both T10 and T22 are recognized equally by 7H9 with a high affinity around 0.1 nM determined by surface plasmon resonance with immobilized 7H9 (*9*).

In B10.BR (H-2$^k$) mice in which the T22 gene is nonfunctional (*10*), cell surface expression of T10 was only observed if splenic cells were activated by LPS or conA. An increase in T10 expression was also observed, after antigenic stimulation, on αβ T cells from B10.BR mice transgenic for the 5CC7 αβ T cell receptor (TCR), which is specific for the cytochrome c–I-E$^k$ (Fig. 1B). The induction of T10 or T22 on splenocytes, including B cells and cells other than B and T cells, has also been observed in a peripheral tolerance induction model (*11, 12*). Because γδ T cells can recognize their ligands directly, without a requirement for antigen processing and presentation, the induction of T10 and T22 on the cell surface of lymphocytes may provide a mechanism by which γδ T cells specific for T10 and/or T22 to regulate immune cells.

If T10 and T22 are biologically important γδ T cell ligands, then the γδ T cells specific for these molecules should be detectable in unimmunized mice. Tetrameric peptide-MHC reagents have been used to track both MHC class I and class II restricted αβ T cell populations (*11, 13*). We therefore used the T22 protein to produce a tetrameric flow cytometry staining reagent (*14*). This reagent stains the G8 hybridoma but not αβ T cell hybridomas or the γδ T cell LBK5 (specific for I-E$^k$) (*9*). Nearly all splenic γδ T cells in G8 γδ TCR transgenic mice were stained by the tetramer (Fig. 2A). Staining of αβ T cells was not observed in either spleen or intestine (*9, 15*).

In normal animals, approximately 0.3 to 0.6% of splenic γδ T cells stained with the tetramer (Fig. 2C) (*16*). Greater than 90% of these cells are CD4$^-$8$^-$, while the rest are either CD4 or CD8 single positive (about 3 to 4% each) (*15*). A similar frequency of tetramer-positive γδ T cells was also found in the intestinal intraepithelial lymphocyte (iIEL) population (*9*). Tetramer binding was abolished when cells were first incubated with monomeric T22-$\beta_2$M (Fig. 2D), further demonstrating the specificity of the tetramer-positive cells for T22. Further, splenic γδ T cells from normal mice activated by plate-bound T22-$\beta_2$M complex, or by Chinese hamster ovary (CHO) cells expressing T10, showed an induced activated phenotype on tetramer-positive, but not on the tetramer-negative cell populations (Fig. 3) (*15*). Taken together, these results demonstrate that a population of γδ T cells in the spleen respond to T22 and/or T10 and that they can be identified by the T22 tetramer staining reagent. It should be noted that MICA/B, human inducible nonclassical MHC class I molecules, have been shown to trigger human γδ T cell lines. Subsequent experiments demonstrated that MICA/B are ligands for the activating natural killer cell receptor NKG2D and that the reactivity of γδ T cell lines to MICA/B-expressing cells is inhibited by antibodies to NKG2D. It was proposed that MICA/B might also act as ligands for the γδ TCR, because antibodies to the receptor also inhibited the reactivity (*17, 18*). A direct interaction between MICA/B

[1]Program in Immunology, [2]Department of Microbiology and Immunology, and [3]Department of Genetics, Stanford University School of Medicine, Stanford, CA 94305, USA. [4]Department of Molecular Biology, The Scripps Research Institute, La Jolla, CA 92037, USA.

*Present address: Howard Hughes Medical Institute, Duke University Medical Center, Durham, NC 27705, USA.
†Present address: Division of Immunology and Cell Biology, John Curtin School of Medical Research, Canberra, ACT, Australia.
‡Present address: Stanford Research Institute, Menlo Park, CA 94025, USA.
§Present address: Department of Pathology, University of California San Francisco School of Medicine, San Francisco, CA 94143, USA.
‖To whom correspondence should be addressed. E-mail: chien@leland.stanford.edu